Super resolution DOA for FMCW automotive radar imaging

Xu, Shengzhi; Wang, Jianping; Yarovoy, Alexander

Citation (APA)
Xu, S., Wang, J., & Yarovoy, A. (2018). Super resolution DOA for FMCW automotive radar imaging. In C. Pichot, M. Lindén, & N. Petrovic (Eds.), *2018 IEEE Conference on Antenna Measurements and Applications, CAMA 2018* Article 8530609 IEEE. https://doi.org/10.1109/CAMA.2018.8530609

Important note
To cite this publication, please use the final published version (if applicable).
Please check the document version above.

Super Resolution DOA for FMCW Automotive Radar Imaging

Shengzhi Xu, Jianping Wang, Alexander Yarovoy
Microwave Sensing, Signals and Systems (MS3)
Delft University of Technology (TU Delft)
2628 CD Delft, the Netherlands
s.xu-4@tudelft.nl, j.wang-4@tudelft.nl, a.yarovoy@tudelft.nl

Abstract—Radar imaging using ultra-wideband (UWB) automotive radar is investigated. To overcome poor cross-range resolution of traditional beamforming (BF) algorithms, super resolution technique is applied for the Direction of Arrival (DOA) estimation. Both super-resolution algorithm and conventional BF method are used to process experimental data collected with UWB frequency modulated continuous wave (FMCW) automotive radar. Algorithm performances are thoroughly compared.

I. INTRODUCTION

Automotive radar has been significantly growing in popularity in recent years [1]. The basic concept of automotive FMCW radar is to generate and transmit a linear frequency ramp as transmit signal. By mixing the transmitted and received signals, the beat frequency signal is generated in the receiver. The range profile is obtained by spectrum analysis of such beat frequency. Meanwhile, the angle profile of the targets could be extracted from the phase delay between different radar antenna array elements. Although with multiple-input-multiple-output (MIMO) radar the equivalent aperture of the virtual array is up to two times larger as the physical aperture, the angular resolution of conventional BF is extremely limited by the number of the elements. To improve the performance of angle-range imaging, so-called super-resolution algorithms, such as 2D multiple signal classification (MUSIC) [2], 3D MUSIC [3] and DFT-ESPRIT [4], have been introduced to automotive radar. However, the high-dimensional MUSIC cannot be adopted for real-time implementation due to the high computational load. Besides, the discrete Fourier transform - estimation of signal parameters via rotational invariance techniques (DFT-ESPRIT) algorithm can hardly work in the challenging environment because the 1D DFT of only one element could not provide sufficient SNR to detect the targets.

To reduce the imaging complexity and at the same time provide high angular resolution, we have presented the DFT combined with MUSIC algorithm for the UWB MIMO automotive radar angle-range imaging and the results from measured data are presented and compared with that of conventional BF method. The data are collected from moving cars equipped with NXP radar demonstrator [5]. After the data preprocess and MIMO calibration, the range profile is processed by DFT for high efficiency and MUSIC algorithm is applied to angle profile for high angular resolution. The spatial smoothing is applied to avoid coherent sources and a dynamic threshold is set to detect the number of the sources in each range cell. Besides, a dynamic normalizer is also applied to each range cell to approximate the true spectrum image [6].

The rest of the paper is organized as follows: Section II describes how the experimental data are collected and preprocessed; the imaging algorithm is described in detail in Section III; the imaging results are presented and compared in Section IV; Main conclusions about the performance are drawn in Section V.

II. DATA COLLECTION AND PREPROCESSING

The experiments are implemented in the campus of Delft University of Technology where there are many stationary parking cars, concrete buildings and moving bicycles. The MIMO radar (see in Fig. 1) is set in the front of a car as shown in Fig. 2. The radar with 3 transmitters and 4 receivers can be considered as the uniformly distributed array with 3×4 elements. The car moved at speed of around 10 Km/h inside the campus. The raw data were collected by radar and the scenarios were captured by the driving recorder (Camera and GPS). The radar system settings are shown in Table
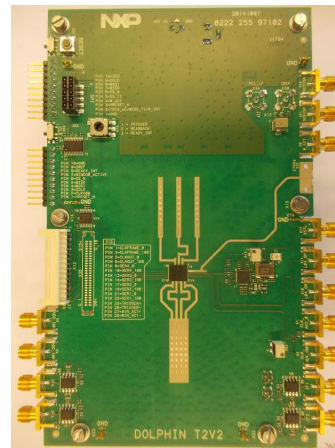

Fig. 1: NXP radar demonstrator RF board

I. The transmitted FMCW signal model is shown in Fig 3. The MIMO transmitters transmit chirp signals sequentially and the reflected signals from the reflector are received by four receivers. After mixing with the transmitted signal, the beat

Fig. 2: Experimental auto equiped with NXP radar demonstrator

TABLE I: System Parameters

Parameters	Values
Center frequency	78.8 GHz
Bandwidth	1 GHz
Number of Transmitters	3
Number of Recievers	4
Number of Pulses	32
Distance between elements	1.899 mm
Sampling Frequency	20 MHz
Chirp Duration	50 μs
Dwell Time	1 μs
Reset Time	5 μs

frequency signal is generated and digitized by sampling at a low sampling rate.. However, the raw data cannot be processed for imaging immediately, and some preprocessing operations should be implemented to filter out the interferences. The original measured data include many interferences due to the system settings. Besides, the array pattern needs to be calibrated to suppress the mutual coupling between array elements.

A. Data Preprocessing

The FMCW signal is illustrated in Fig. 3. The t_{dwell} in Fig. 3 is the time preparing to transmit frequency-modulated signal. After the frequency reaches the maximum value, t_{reset} is needed to reset the frequency to starting frequency. Thus, the beat signal in these durations contain no useful information and have to be removed. Besides, the t_{settle} is the initial time of modulation which could be nonlinear and unstable and have to be removed. The only useful data are collected in the time periods which are shown as the green line in Fig. 3.

B. MIMO Calibration

The MIMO calibration vector is collected by experimental trials. The steering vector directing to angle θ of MIMO virtual array is $\mathbf{a}(\theta) = \boldsymbol{\alpha}(\theta) \otimes \boldsymbol{\beta}(\theta)$, where $\boldsymbol{\alpha}(\theta)$ is the transmitted steering vector, $\boldsymbol{\beta}(\theta)$ is the recieved steering vector and $\otimes$ denotes the Kronecker product. In the following, the virtual array steering vector $\mathbf{a}(\theta)$ will be adopted. The signal reflection of a single target located in the $0°$ is collected in the laboratory as $\mathbf{a}_{\text{measured}}(0°)$. The ideal reflection of such target
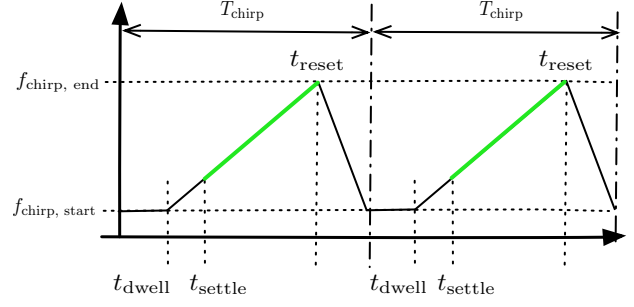

Fig. 3: FMCW Signal Model

without mutual coupling is calculated as $\mathbf{a}_{\text{ideal}}(0°)$. Then the calibration vector for this angle can be approximated by

$$\mathbf{c} = \mathbf{a}_{\text{ideal}}(0°) \oslash \mathbf{a}_{\text{measured}}(0°) \tag{1}$$

where $\oslash$ denotes the elementwise division. Then the raw data can be calibrated by taking elementwise production with $\mathbf{c}$ along the virtual array dimension. After all the pre-processing. the three-dimensional beat frequency data model $\boldsymbol{\mathcal{Y}} \in \mathbb{C}^{L \times M \times K}$ can be written as

$$\boldsymbol{\mathcal{Y}} = \sum_{i=1}^{I} \alpha_i \mathbf{a}(\theta_i) \circ \mathbf{f}_i^d \circ \mathbf{f}_i^r + \boldsymbol{\mathcal{N}} \tag{2}$$

where $\circ$ denotes the outer product, $i = 1, 2, ..., I$ is the index of the far-field targets, α denotes the complex amplitude, L denotes the number of elements of the virtual array, M denotes the number of the chirps, K denotes the number of fast time samples after preprocessing, θ_i denotes the angle of the ith scatterer, $\boldsymbol{\mathcal{N}} \in \mathbb{C}^{L \times M \times K}$ denotes the additive system noise, and $\mathbf{a}(\theta_i) \in \mathbb{C}^{L \times 1}$, $\mathbf{f}_i^d \in \mathbb{C}^{M \times 1}$, $\mathbf{f}_i^r \in \mathbb{C}^{K \times 1}$, respectively, denote the virtual steering vector, Doppler beat frequency vector, range beat frequency vector of the ith scatterer. Here, according to the system parameters, the range migration phenomenon of slowly moving targets is nonobvious and could be neglected in the model.

III. IMAGING FOR ANGLE-RANGE

After removing the interferences and array calibration, the data are prepared for imaging. The UWB signal provides sufficiently high range resolution with DFT. Thus, DFT is directly applied to the range domain. To accurately indicate the range profile, zero-padding is made before the fast Fourier transform (FFT) operation. After 1D FFT, the data model $\mathbf{Y}_{\tilde{k}} \in \mathbb{C}^{L \times M}$ of the $\tilde{k}$th range cell can be written as

$$\mathbf{Y}_{\tilde{k}} = \sum_{i=1}^{I} \text{sinc}(\beta(r_{\tilde{k}} - r_i)) \times \mathbf{a}(\theta_i)(\mathbf{f}_i^d)^T + \mathbf{N} \tag{3}$$

where sinc() is the sinc function, $(\cdot)^T$ means transpose of the matrix, β is a constant determined by the system parameters, $\tilde{k}$ is the index of the range profile after FFT, r_i is the range of ith scatterer and $\mathbf{N}$ is the noise matrix. As for the angle domain, 1D MUSIC is applied for each range cell by using the Doppler beat frequency dimension as the reference dimension.

A. Spatial Smoothing

Spatial smoothing has to be implemented before applying MUSIC algorithm in each range cell to separate the coherent signals. In fact, two closely spaced stationary targets have almost the same Doppler shift and are hardly separated by eigendecomposition. For a detailed explanation of spatial smoothing, the reader is referred to [7].

B. Targets Detection in Each Range Cell

The eigendecomposition is performed then to the smoothed covariance matrix $\mathbf{C}_{\tilde{k}} \in \mathbb{C}^{(L-P)\times(L-P)}$ to obtain the eigen space as

$$\mathbf{C}_{\tilde{k}} = \mathbf{U}_{\tilde{k}}\boldsymbol{\Lambda}_{\tilde{k}}\mathbf{U}_{\tilde{k}}^H \tag{4}$$

Where P is the constant for dimension reduction in spatial smoothing, $\mathbf{U}_{\tilde{k}}$ is the unitary matrix. The eigenvalues can be found from the diagonal matrix $\boldsymbol{\Lambda}$. The eigenvalue vector is

$$\boldsymbol{\lambda}_{\tilde{k}} = [\lambda_{\tilde{k},1}, \lambda_{\tilde{k},2}, ..., \lambda_{\tilde{k},L-P}] = \mathrm{diag}(\boldsymbol{\Lambda}) \tag{5}$$

where diag() is the the operation to get the diagonal elements of a matrix. The number of the targets can be estimated from the such vector. If there is no noise, the absolute values of the eigenvalues decrease very smoothly. While if there are some targets presented, the absolute value of the eigenvalues corresponding to the targets will be much larger than that corresponding to the noise. Thus, a threshold can be defined from the eigenvalue vector to estimate the number of targets in this range cell.

C. MUSIC Algorithm for Angle-Range Imaging

Then according to the number of the detected targets, the noise subspace can be extracted from the eigendecomposition as

$$\mathbf{U}_{\tilde{k}} = [\mathbf{W}_{\tilde{k}}\ \mathbf{V}_{\tilde{k}}] \tag{6}$$

where $\mathbf{W}_{\tilde{k}}$ and $\mathbf{V}_{\tilde{k}}$ represent the signal subspace and noise subspace, respectively. Divide the angle domain into Q grids as $[\theta_0, \theta_1, ..., \theta_Q]$ and formulate the steering vector $\mathbf{a}(\theta) \in \mathbb{C}^{(L-I)\times 1}$ as

$$\mathbf{a}(\theta) = [1, e^{j2\pi\frac{d}{\lambda}\sin\theta}, ..., e^{j2\pi\frac{(L-P)d}{\lambda}\sin\theta}]^T \tag{7}$$

where d is the inter space between neighbouring virtual elements and λ is the wavelength of the center frequency. Applying MUSIC algorithm, the pseudo-spectrum of angle $\mathbf{p}_{\tilde{k}} \in \mathbb{R}^{Q\times 1}$ can be obtained

$$\mathbf{p}_{\tilde{k}} = [\frac{1}{||\mathbf{a}(\theta_0)\mathbf{V}_{\tilde{k}}||^2}, ..., \frac{1}{||\mathbf{a}(\theta_Q)\mathbf{V}_{\tilde{k}}||^2}]^T \tag{8}$$

The MUSIC spectrum is the pseudo-spectrum, which means the amplitudes of MUSIC results cannot directly represent the amplitudes of scatterers. The pseudo-spectrum is normalized to the same baseline in different range cells. and then the spectral norm of the $\mathbf{Y}_{\tilde{k}}$ is used to approximately represent the relative spectrum.

IV. PROCESSING RESULTS

In this section, we will present some results of the measured data by the proposed methods. The car was moving with speed of about 10 Km/h for the whole experiment.

The first scenario for the measured data is shown in Fig. 4(a), where the strong reflectors contain the building wall with metal reinforcement (indicated by the purple dashed line), a pedestrian close to the wall (indicated by the green circle), a metal sewer cover (indicated by green circle) some stationary cars (indicated by red circle). The imaging result of the proposed method for such scenario is shown in Fig. 4(c), and for comparison, the processing results using conventional BF method is shown in Fig. 4(b). By comparison, the spectra of the wall metal reinforcement and the car are narrower for super-resolution algorithm than that of BF method. Moreover, the pedestrian and sewer cover are masked by the sidelobes of the spectra of the wall in Fig. 4(b), while in Fig. 4(c) the pedestrian and the sewer cover can be clearly separated from the wall (indicated by the white arrows).

The second scenario is shown in Fig. 5(a), where the strong reflectors are the bicycles along the road (indicated by the purple dashed line), a cyclist (indicated by the green circle) and a lamppost (indicated by the cyan square) in front of the car. The processing results using both MUSIC algorithm and BF method are show in Fig. 5(c) and Fig. 5(b), respectively. The figures also show that the spectrum for both bicycles and lamppost are overall narrower and more clear of MUSIC algorithm than that of BF method. The sidelobes for BF method (indicated with red arrows) are as strong as the spectrum of the cyclist (indicated with the white arrow), which makes it difficult to identify the cyclist.

From the figures and analysis above, the performance of the angular resolution of MUSIC algorithm is overall much better than that of the BF method. The time consumption of two methods for the same data and with the same computer is 0.44 second for the DFT-MUSIC method and 0.09 second for DFT-BF method. Although it is slightly slower in this case, the proposed DFT-MUSIC algorithm has much room for efficient implementation by using parallel processing in the real application.

V. CONCLUSIONS

In this paper, we have presented UWB MIMO automotive radar angle-range imaging using DFT-MUSIC and the results with experimental data. The data collected from moving cars are preprocessed and calibrated at first. Then the DFT-MUSIC algorithm is applied for the angle-range imaging. The range profile is processed by DFT for efficiency and MUSIC algorithm is applied for angle profile for high-resolution separation. The experimental results obtained with MUSIC and BF method are presented and compared. Although the time consumption is slightly increased, it is clear that MUSIC algorithm provides much higher angular resolution without strong side lobes.
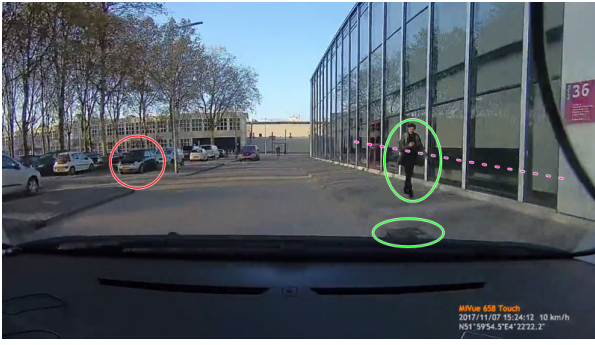
(a)
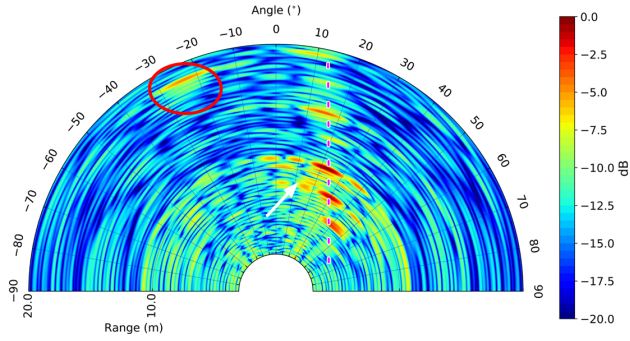
(b)
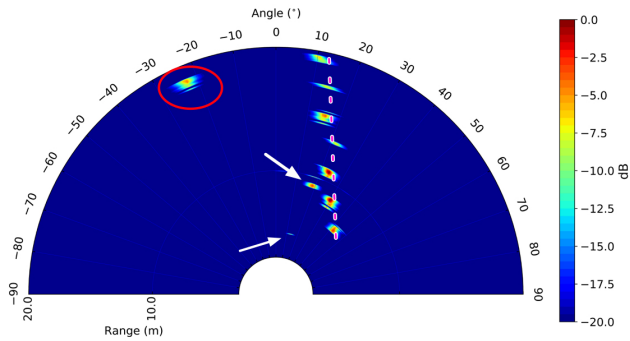
(c)

Fig. 4: Scenario 1: (a) the scenario captured by camera; (b) the results of DFT-BF method; (c) the results of DFT-MUSIC method
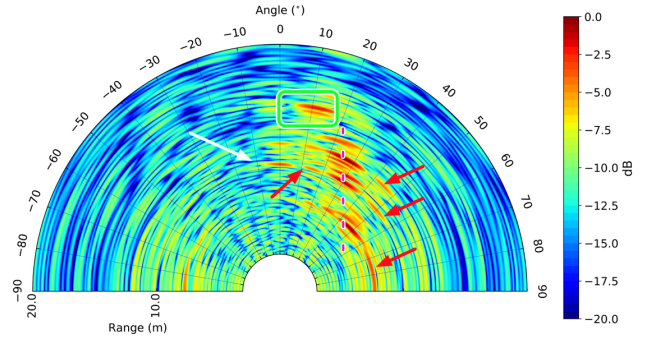

(a)

(b)

(c)

Fig. 5: Scenario 2: (a) the scenario captured by camera; (b) the results of DFT-BF method; (c) the results of DFT-MUSIC method
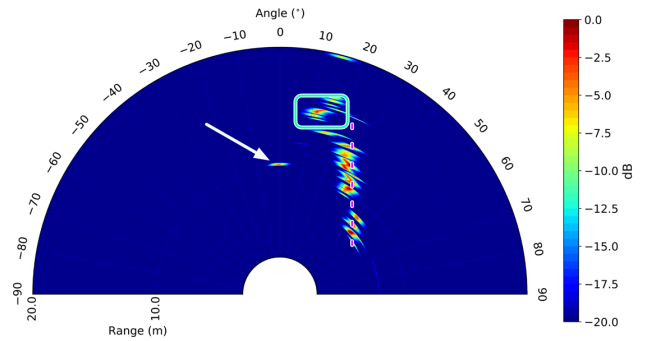
REFERENCES

[1] I. Shapir, I. Bilik, and G. Barkan, "Doppler ambiguity resolving in tdma automotive mimo radar via digital multiple prf," in *2018 IEEE Radar Conference (RadarConf18)*, April 2018, pp. 0175–0180.

[2] S. Xu and A. Yarovoy, "Joint doppler and doa estimation using 2d music in presence of phase residual," in *2017 European Radar Conference (EURAD)*, Oct 2017, pp. 203–206.

[3] Y. Gürcan and A. Yarovoy, "Super-resolution algorithm for joint range-azimuth-doppler estimation in automotive radars," in *2017 European Radar Conference (EURAD)*, Oct 2017, pp. 73–76.

[4] S. Kim, D. Oh, and J. Lee, "Joint dft-esprit estimation for toa and doa in vehicle fmcw radars," *IEEE Antennas and Wireless Propagation Letters*, vol. 14, pp. 1710–1713, 2015.

[5] [Online]. Available: https://www.nxp.com/

[6] S. Xu, J. Wang and A. Yarovoy. "Joint dft-music estimation for toa and doa in vehicle fmcw radar," in prep.

[7] F. Belfiori, W. van Rossum, and P. Hoogeboom, "2d-music technique applied to a coherent fmcw mimo radar," in *IET International Conference on Radar Systems (Radar 2012)*, Oct 2012, pp. 1–6.